Inorganic Chemistry

pubs.acs.org/IC Article

Chemoselectivity for B−O and B−H Bond Cleavage by Pincer-Type Phosphorus Compounds: Theoretical and Experimental Studies

Qin Zhu,[‖] Penglong Wang,[‖] Jun Zhu,* Congqing Zhu,* and Guixiang Zeng*

Cite This: *Inorg. Chem.* 2020, 59, 15636−15645 Read Online

ACCESS | Metrics & More | Article Recommendations | Supporting Information

ABSTRACT: Selective cleavage of the B−O bond or B−H bond in HBpin can be achieved by adjusting the pincer ligand of a phosphorus(III) compound guided by a combination of theoretical prediction and experimental verification. Theoretical calculations reveal that a pincer-type phosphorus compound with an $[ONO]^{3-}$ ligand reacts with HBpin, leading to cleavage of the stronger B−O bonds ($\Delta G^{\circ\ddagger}$ = 23.2 kcal mol^{-1}) rather than the weaker B−H bond ($\Delta G^{\circ\ddagger}$ = 26.4 kcal mol^{-1}). A pincer-type phosphorus compound with a $[NNN]^{3-}$ ligand reacts with HBpin, leading to the weaker B−H bond cleavage ($\Delta G^{\circ\ddagger}$ = 16.2 kcal mol^{-1}) rather than cleavage of the stronger B−O bond ($\Delta G^{\circ\ddagger}$ = 33.0 kcal mol^{-1}). The theoretical prediction for B−O bond cleavage was verified experimentally, and the final products were characterized by NMR, HRMS, and single-crystal X-ray diffraction. The chemoselectivity of B−O bond cleavage was also observed in the presence of B−C or B−B bonds in borane substrates.

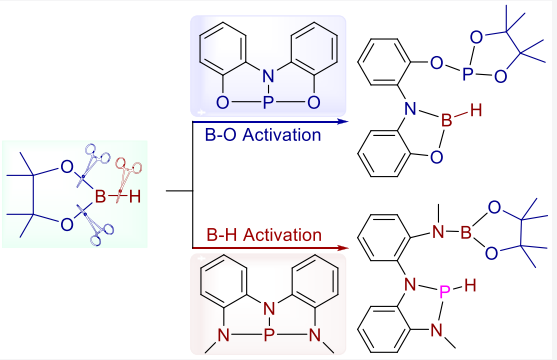

INTRODUCTION

The formation and cleavage of chemical bonds are fundamental concepts in chemistry. Selective activation or cleavage of chemical bonds provides a green approach to the synthesis of value-added products and could revolutionize chemical synthesis by creating completely new synthetic strategies.[1−4] Much progress has been made in the activation of chemical bonds by d-block transition-metal complexes,[5−8] but transition metals are usually expensive and environmentally unfriendly, and their use increases the cost of chemical syntheses. Replacing the d-block transition metals with the p-block main-group elements, which are cheap, abundant, and environmentally friendly, is a promising way to solve these problems.[9−12] In this context, a variety of compounds containing main-group elements including carbone and carbene,[13−17] low-valent species of group 13−15 elements,[18−22] and frustrated Lewis pairs (FLPs)[23−26] have been reported.

In the past few decades, a series of pincer-type phosphorus compounds have been reported.[27−43] For example, Arduengo and co-workers found that the main-group phosphorus compound (**I**) facilitates the activation of RO−H bonds (Chart 1A).[27,28] This study has been extended to geometrically constrained phosphorus system (**II**)[31−33] and nonplanar phosphorus triamide (**III**)[34−38] by the groups of Goicoechea and Radosevich, respectively. Such phosphorus compounds were found to be capable of activation of σ bonds, such as N−H, O−H, or B−H. It has been shown theoretically and experimentally that the electronics of the backbone of the pincer ligand plays a crucial role in these reactions. Of the σ-bond activations, the B−H bond activation is particularly attractive because the boron unit can be easily transformed to another functional group and substituted borane compounds have unique applications in Suzuki−Miyaura coupling reactions.[44−47] The activation of the H−Bpin bond by a nonplanar phosphorus triamide (**III**) was reported by Radosevich et al. in 2017 (Chart 1B).[38] This reaction was followed by the hydroboration of imines to regenerate the catalyst, completing the catalytic cycle. Hereafter, the triamide ligand is represented by $[NNN]^{3-}$. According to our previous theoretical works,[48,49] substituting the $[NNN]^{3-}$ ligand for an $[ONO]^{3-}$ ligand should improve the activity of the pincer-type phosphorus compound in the activation of σ bonds. In view of the importance of pincer ligands in these reactions, a deep understanding of their reactivity is necessary to expand their diversity.

We studied theoretically the detailed mechanisms of cleavage of the B−H and B−O bonds in HBpin by compounds **II** (**1**) and **III** (**2**) and found that compound **1** with an $[ONO]^{3-}$ ligand exclusively promotes the activation of the stronger B−O bond over the weaker B−H bond in such reactions (Chart 1C). This was further confirmed experimentally. Our research provides a fundamental investigation of the chemoselective activation of B−E bonds by main-group pincer-type phosphorus compounds.

Received: June 29, 2020
Published: October 20, 2020

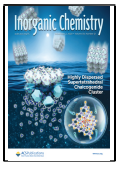

https://dx.doi.org/10.1021/acs.inorgchem.0c01920
Inorg. Chem. 2020, 59, 15636−15645

Chart 1. σ-Bond Activation by Pincer-Type Phosphorus Compounds

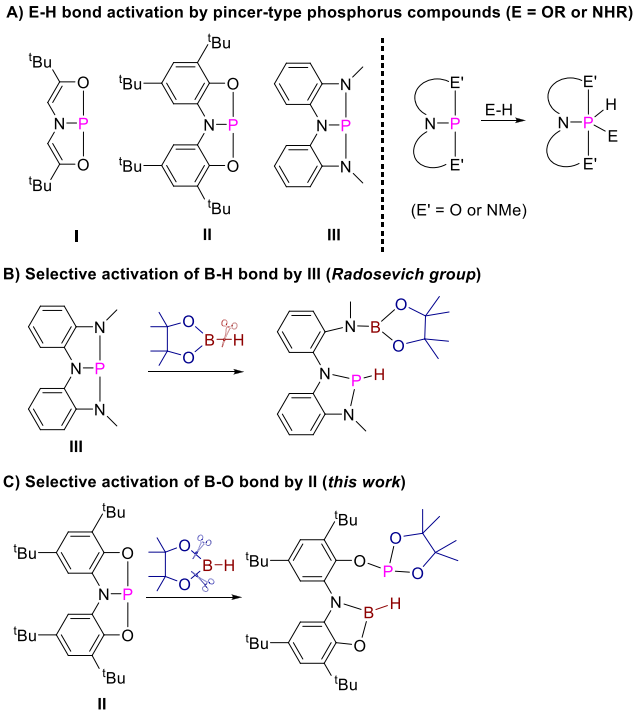

COMPUTATIONAL DETAILS

All of the geometries were fully optimized by the density functional theory (DFT) method with the B3PW91 density functional in solution (benzene),[50,51] where the empirical dispersion (D3) was considered.[52] The solvent effect was considered with the conductor-like polarizable continuum model (CPCM).[53,54] Harmonic frequency calculations were performed for each stationary structure to determine whether it is an equilibrium structure (no imaginary frequencies) or a transition state (one imaginary frequency). Calculations of the intrinsic reaction coordinates (IRC) were carried out for each transition state to determine whether or not it connects the reactant with the product in a specific reaction step.[55,56] In the calculations, the 6-31+G(2d) basis set[57,58] was used for the phosphorus atom and the 6-31+G(d,p) basis sets[59] were employed for the other atoms. All of these calculations were carried out by the Gaussian 16 program.[60] The Gibbs activation energy ($\Delta G^{\circ\ddagger}$) of a reaction was calculated as the difference in Gibbs energy between the transition state (TS) and the most stable species, reactant or intermediate, before the TS. The Gibbs reaction energy (ΔG°) was calculated as the Gibbs energy difference between the product and the reactant in a specific step.

RESULTS AND DISCUSSION

HBpin Activation by $[ONO]^{3-}$ Ligand Supported Phosphorus Compound 1. In HBpin activation, compound **1**[31] transforms from a bent structure to a planar structure (**1′**), which is 2.1 kcal mol^{-1} less stable (Figure 1). HBpin then associates with **1′** to form **3** via the transition state $\mathbf{TS_{1'/3}}$, with $\Delta G^{\circ\ddagger}$ and ΔG° values of 19.2 and 10.0 kcal mol^{-1}, respectively. When the reaction proceeds from $\mathbf{TS_{1'/3}}$ to **3**, the B−O1 distance significantly decreases from 1.964 to 1.477 Å (Figure 2), indicating that a bond has been formed between B and O1. In the meanwhile, O3 approaches the P atom, leading to a large elongation of the B−O3 bond by 0.179 Å. Due to these geometrical changes, the B−H bond in the HBpin moiety in **3** becomes slightly longer by 0.016 Å.

With **3** as the starting point, there are two possibilities. One is B−H bond activation, which occurs through the transition state $\mathbf{TS_{3/4\text{-}BH}}$ to produce **4-BH**, as shown by a red line in Figure 1. When the reaction proceeds from **3** to $\mathbf{TS_{3/4\text{-}BH}}$, the HBpin moiety rotates along the B−O1 bond in order to bring the B−H bond close to the phosphorus center (Figure 2). With this rotation, the dihedral angle ∠H−B−O1−P decreases from 101.4° to 55.9°, and the P−H1 distance is significantly shortened by 0.772 Å. At the same time, the B−H bond is moderately elongated from 1.208 to 1.244 Å. In **4-BH**, the distance between B and H is elongated to 2.590 Å and the P−H distance is shortened to 1.439 Å, indicating that the B−H bond

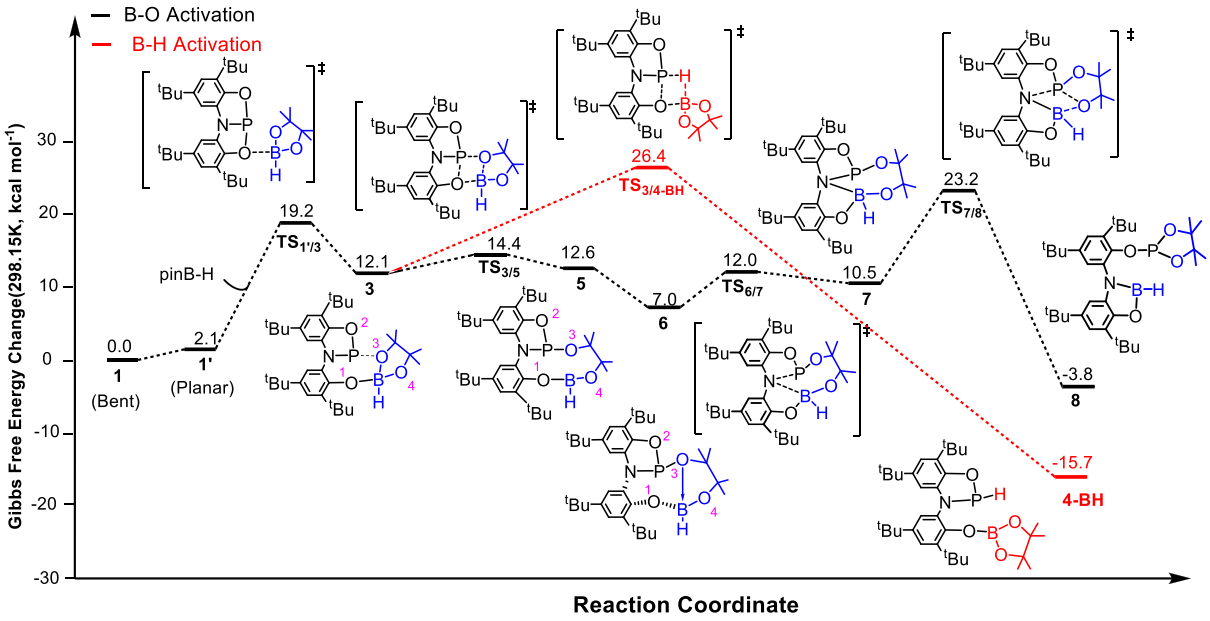

Figure 1. Calculated Gibbs energy profiles for the B−O bond and B−H bond activation in HBpin by **1**. The atom numbers of different oxygens are given in purple.

https://dx.doi.org/10.1021/acs.inorgchem.0c01920
Inorg. Chem. 2020, 59, 15636−15645

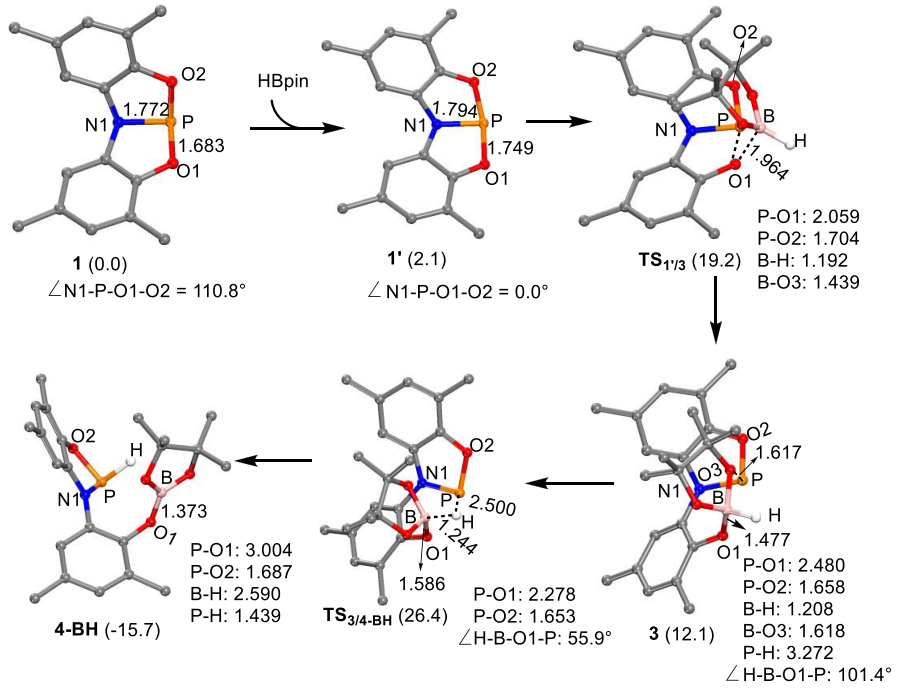

Figure 2. Theoretical optimized geometries for all species along the B−H bond activation by **1**. Methyl groups in ^{t}Bu and some hydrogen atoms are omitted for clarity. Distances are given in Å. Gibbs energy changes are given in parentheses in kcal mol^{-1}.

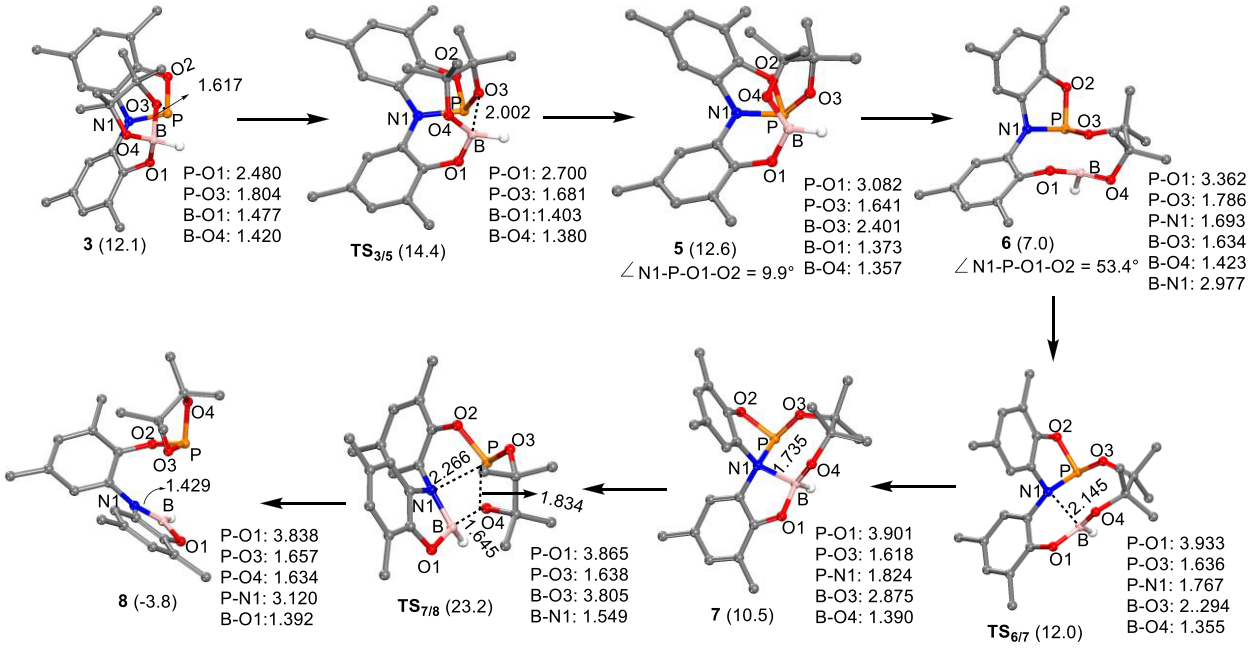

Figure 3. Theoretical optimized geometries for all species along the B−O bond activation by **1**. The methyl group in ^{t}Bu and some hydrogen atoms are omitted for clarity. Distances are given in Å. Gibbs energy changes are shown parenthetically in kcal mol^{-1}.

has been broken and a P−H bond has been formed. The $\Delta G^{\circ\ddagger}$ and ΔG° values of this step are 26.4 and −27.8 kcal mol^{-1}, respectively.

Another possible reaction pathway involves B−O bond activation. As shown in Figure 1, the B−O3 bond activation occurs through $\mathbf{TS}_{3/5}$ to afford **5** (black line), in which the phosphorus center and the $[ONO]^{3-}$ ligand can be cooperative. The $\Delta G^{\circ\ddagger}$ value of this step is 14.4 kcal mol^{-1}, which is much lower than that of B−H bond activation (26.4 kcal mol^{-1}). This indicates that the B−O3 bond activation is much more facile than the B−H bond activation. In this step, the B−O3 activation is slightly endothermic by 0.5 kcal mol^{-1} due to the steric repulsion between the pincer ligand and the diolate ligand (in the *syn* form) in **5**. Compound **5** easily transforms to a more stable species (**6**), in which the diolate ligand and the pincer ligand are in an *anti* orientation. This transformation reaction is exothermic by 5.6 kcal mol^{-1}.

Nucleophilic attack of the chelating atom N1 of the $[ONO]^{3-}$ ligand to the boron atom through $\mathbf{TS}_{6/7}$ affords **7** (Figure 1). This process occurs easily and has $\Delta G^{\circ\ddagger}$ and ΔG° values of 12.0

https://dx.doi.org/10.1021/acs.inorgchem.0c01920
Inorg. Chem. 2020, 59, 15636−15645

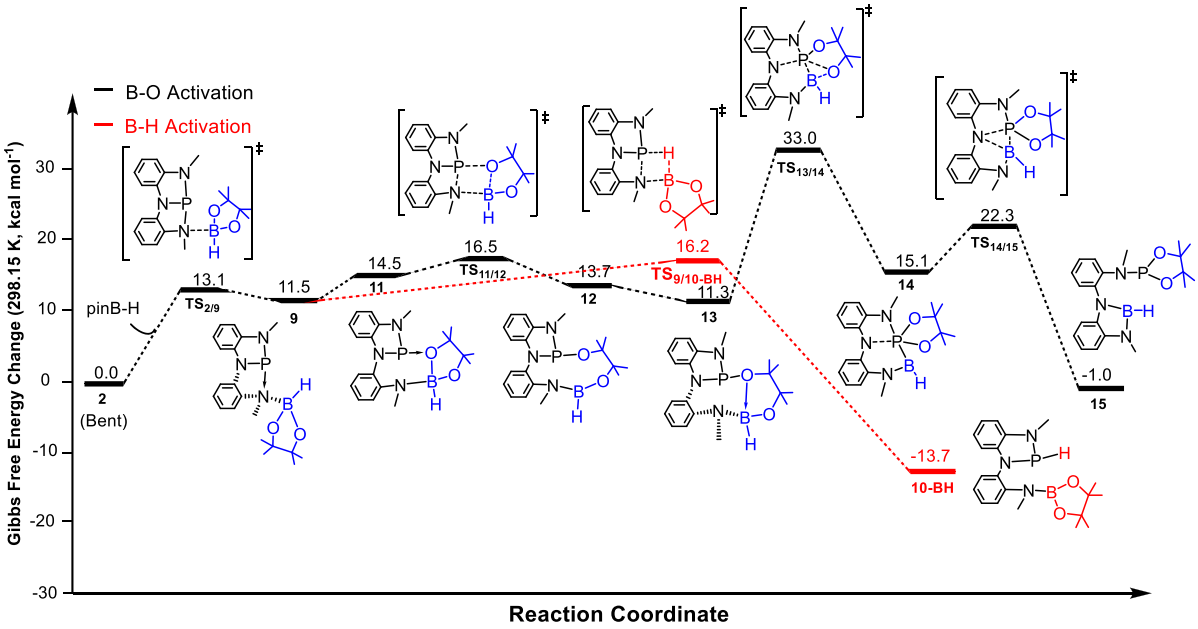

Figure 4. Calculated Gibbs energy profiles for the B−O bond and B−H bond activation in HBpin by **2**.

and 3.5 kcal mol^{-1}, respectively. Next, compound **8** is formed by the second B−O bond cleavage. This step takes place through $\mathbf{TS}_{7/8}$, in which the B−O4 and P−N1 bond distances increase to 1.645 and 2.266 Å, respectively, and as a result, the P−O4 and B−N1 distances are shortened to 1.834 and 1.549 Å, respectively (Figure 3). The $\Delta G^{\circ\ddagger}$ and ΔG° values of this step are 23.2 and −14.3 kcal mol^{-1}, respectively, indicating that the reaction is both thermodynamically and kinetically favorable. On the other hand, the second B−O bond activation was achieved by the nucleophilic attack of phosphorus to the boron in compound **6**. This pathway requires a moderate higher energy for the rate-determining step (RDS) (30.7 kcal mol^{-1}, Figure S1), which has difficulty in occurring in experiments.

In the reaction of HBpin with the pincer-type phosphorus compound **1** activation of the B−O bond ($\Delta G^{\circ\ddagger}$ = 23.2 kcal mol^{-1} for the RDS) is therefore preferred over B−H bond activation ($\Delta G^{\circ\ddagger}$ = 26.4 kcal mol^{-1}). However, the final product (**8**) of the B−O activation is less stable than **4-BH** (the product of B−H bond activation, Figure 1) by 11.9 kcal mol^{-1}, which indicates that the activation of the B−O bond is preferred kinetically.

HBpin Activation by [NNN]$^{3-}$ Ligand Supported Phosphorus Compound 2. In order to explore the ligand influence on the reactivity, we investigated the reaction of HBpin with **2**, which carries a [NNN]$^{3-}$ ligand.[38] This reaction is initiated by the coordination of HBpin with **2** (Figure 4). This step proceeds through $\mathbf{TS}_{2/9}$ to afford the intermediate **9**, where the $\Delta G^{\circ\ddagger}$ and ΔG° values are 13.1 and 11.5 kcal mol^{-1}, respectively.

For the B−H bond activation, which occurs through $\mathbf{TS}_{9/10\text{-BH}}$ to produce a hydride phosphine compound (**10-BH**) with a pendant borane unit, see the red line in Figure 4. In this step, the phosphorus center and the amine unit work cooperatively. The $\Delta G^{\circ\ddagger}$ and ΔG° values of this step are 16.2 and −25.2 kcal mol^{-1}, respectively, indicating the B−H bond activation occurs easily (see Figure S2 for geometry changes).

The other possible reaction starting from **9** is the B−O bond activation (black line in Figure 4). First, **9** is transformed to the unstable species **11**, in which the HBpin moiety rotates along the B−N1 axis to bring the B−O bond toward the phosphorus center. This step is endothermic by 3.0 kcal mol^{-1}. Then, the first B−O bond cleavage by the phosphorus center through $\mathbf{TS}_{11/12}$ affords **12**, and the $\Delta G^{\circ\ddagger}$ and ΔG° values are 16.5 and −0.8 kcal mol^{-1}, respectively. Compound **12** is not a stable intermediate and is easily isomerized to **13** with a ΔG° value of −2.4 kcal mol^{-1}. Subsequently, the second B−O bond is cleaved through $\mathbf{TS}_{13/14}$ to form a phosphorus pinacolato compound (**14**). In this step, the reaction took place by insertion of a phosphorus atom into the B−O bond. Compound **14** takes a pentacoordinate (σ^5-P) geometry. The $\Delta G^{\circ\ddagger}$ and ΔG° values for the second B−O bond activation are 33.0 and 3.8 kcal mol^{-1}, respectively, indicating that this is the RDS for the B−O bond activation. In the final step, compound **15** is generated through $\mathbf{TS}_{14/15}$. The $\Delta G^{\circ\ddagger}$ and ΔG° values for this step are 22.3 and −16.1 kcal mol^{-1}, respectively, indicating that the reaction is thermodynamically favorable (see Figure S3 for geometry changes). In addition, the N1 nucleophilic attack pathway was also investigated (Figure S4). The RDS of this pathway is 33.3 kcal mol^{-1}, which is less favorable than P nucleophilic attack pathway (33.0 kcal mol^{-1}). The above discussion indicates that B−H bond activation by the [NNN]$^{3-}$ ligand supported pincer-type phosphorus compound **2** is the more favorable than B−O bond activation (Figure 4), which is consistent with the experimental results.[38] Such chemoselectivity is different from the reaction between HBpin with the [ONO]$^{3-}$ ligand supported pincer-type phosphorus compound **1** (Figure 1).

Origin of the Selective Activation of the B−O Bond over the B−H Bond by 1. To shed light on the reason for the selective activation of the B−O bond over the B−H bond by **1**, charge decomposition analyses (CDA) were performed on the transition states $\mathbf{TS}_{3/4\text{-BH}}$ (B−H bond activation) and $\mathbf{TS}_{3/5}$ (B−O bond activation).[61] Generally, MOs of a total system AB can be represented by a linear combination of MOs of fragments A and B (see eq 1)

$$\phi_i(\mathrm{AB}) = \sum_m C_{im}^{\mathrm{A}}\phi_m(\mathrm{A}) + \sum_n C_{in}^{\mathrm{B}}\phi_n(\mathrm{B}) \quad (1)$$

https://dx.doi.org/10.1021/acs.inorgchem.0c01920
Inorg. Chem. 2020, 59, 15636−15645

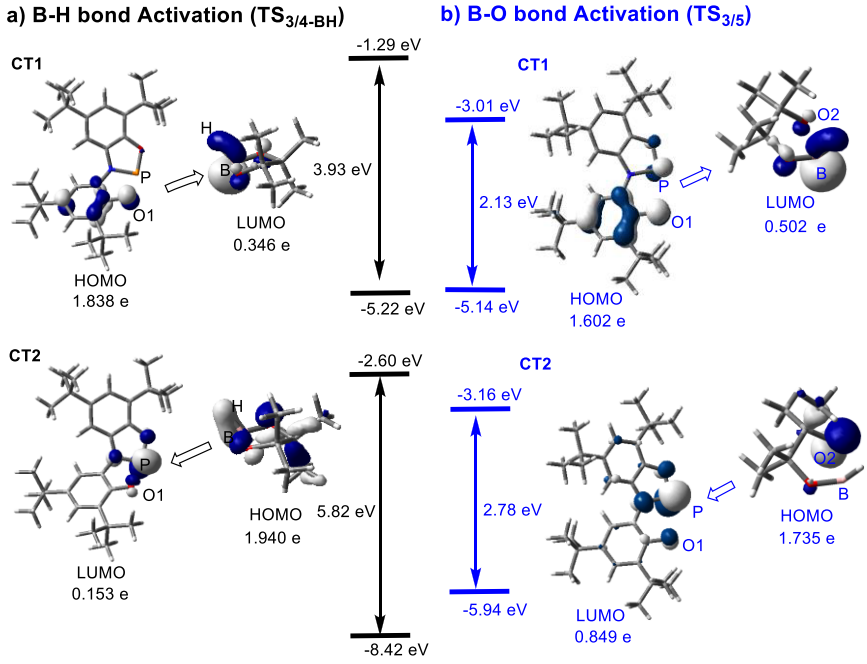

Figure 5. Key molecular orbitals and their occupations in important charger transfer interactions in $\mathbf{TS_{3/4}}$**-BH** for B−H activation and $\mathbf{TS_{3/5}}$ for B−O bond activation by **1**. Molecular orbital energies are provided below and above the bars, and orbital energy gaps are provided beside the double-headed arrows.

where φ_i(AB) represents the ith MO of the complex AB, $\varphi_m(A)$ and $\varphi_n(B)$ are the mth MO and nth MO of fragments A and B, respectively, and C_{im}^{A} and C_{in}^{B} are the expansion coefficients of φ_m(A) and φ_n(B), respectively. The populations of φ_m(A) and φ_n(B) can be obtained from these coefficients C_{im}^{A} and C_{in}^{B}. In these analyses, $\mathbf{TS_{3/4\text{-}BH}}$ and $\mathbf{TS_{3/5}}$ were separated into two moieties, distorted **1** and HBpin. The orbital energies and corresponding orbital populations of molecular orbitals that take part in the charge transfer processes were provided in Figure 5.

In $\mathbf{TS_{3/4\text{-}BH}}$, the populations on the empty p orbital (the LUMO of the HBpin moiety) are the B atom considerably increased to 0.346 e, as shown in Figure 5a. Meanwhile, populations on the HOMO of the **1** moiety, which mainly lies on the *tert*-butylphenoxy group moderately decrease to 1.838 e. This indicates that the charge transfer occurs mainly from the *tert*-butylphenoxy group in **1** to the empty p orbital of the B atom in HBpin (CT1). On the other hand, the populations of the B−H σ-bonding orbital (HOMO of the HBpin moiety) decrease to 1.940 e and that of the P−O π^* orbital (LUMO of the **1** moiety) increases to 0.153 e. This suggests that the charge transfer (CT2) occurs from the B−H σ-bonding orbital to the P−O π^* antibonding orbital of **1**. Both of those CTs contribute to a weakening of the B−H σ bond. CT1 (0.346 e) is clearly much larger than CT2 (0.153 e), indicating that the former plays a dominant role in the B−H bond activation.

In $\mathbf{TS_{3/5}}$, CT1 occurs mainly from the P−O π-bonding orbital (HOMO) of **1** to the B−O π^*antibonding orbital (LUMO of the HBpin moiety), and the empty p orbital of B is the main component (Figure 5b). As a result of CT1, the population of the B−O π^* antibonding orbital increases significantly to 0.502 e and the populations of the P−O π-bonding orbital of **1** decrease considerably to 1.602 e. On the other hand, CT2 occurs from the occupied p orbital of the O atom (HOMO) in the HBpin moiety to the P−O π^* antibonding orbital (LUMO) of **1**. In this process, the populations of the p orbital of the O atom in the HBpin moiety decrease to 1.735 e and the populations on the P−O π^* antibonding orbital of **1** increase to 0.849 e. As shown in Figure 5b, CT2 (0.849 e) is much larger than CT1 (0.502 e), which plays a crucial role in the B−O bond activation.

On comparison of the CTs in Figure 5, both CT1 and CT2 in the B−O bond activation are much larger than those in the B−H bond activation, which makes the cleavage of the B−O bond easier in comparison to that of the B−H bond. This is because the HOMO−LUMO gaps in CT1 (2.13 eV) and CT2 (2.78 eV) are much smaller in $\mathbf{TS_{3/5}}$ in comparison to those in $\mathbf{TS_{3/4\text{-}BH}}$ (3.93 and 5.82 eV, respectively). MO analyses of the transition state for the B−H bond ($\mathbf{TS_{9/10\text{-}BH}}$) and B−O bond ($\mathbf{TS_{11/12\text{-}BH}}$) activation by compound **2** were also computed (see Figures S5 and S6). The electronic process of the B−H bond and B−O bond cleavages of HBpin by **2** are consistent with the electron process of compound **1**, suggesting that electron transfer from **2** to HBpin plays a dominant role in the B−H bond cleavage. Conversely, the electron transfer from HBpin to compound **2** plays a dominant role in the B−O bond cleavage.

To probe the origins of the chemoselectivity, we investigated the global electrophilicity (ω°) and the global nucleophilicity (N°) of **1** and **2**. As shown in Table 1, the global electrophilicity of **1′** is 1.44 eV while the ω° value of **2** is 0.67 eV, suggesting that **1′** is a stronger electrophile than compound **2** and compound **1′** prefers to activate the B−O bond rather than the B−H bond.

Experimental Results. To verify the calculated results, we examined the reaction of compound **1** with HBpin (Scheme 1).

Table 1. Calculated Global Electrophilicity ω° and Global Nucleophilicity N° (in eV) for 1, 1′, and 2

reactivity index	1	1′	2
ω°	1.01	1.44	0.67
N°	3.60	3.35	4.18

https://dx.doi.org/10.1021/acs.inorgchem.0c01920
Inorg. Chem. 2020, 59, 15636−15645

Scheme 1. B−O Bond Activation by 1 in the Presence of a B−H Bond

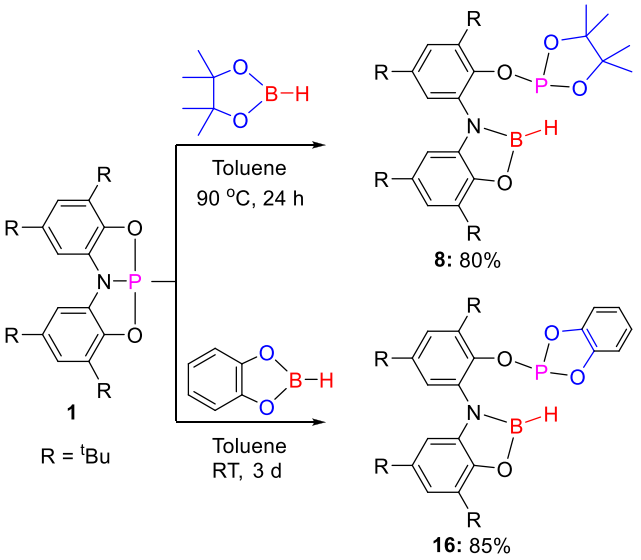

On the basis of the *in situ* $^{31}P\{^{1}H\}$ NMR spectrum, a new single peak at δ 143.6 ppm appeared slowly after **1** was mixed with HBpin at 90 °C. Compound **1** was completely consumed after 24 h, and after workup, **8** was isolated in 80% yield.

Both the $^{31}P\{^{1}H\}$ and ^{31}P NMR spectra of **8** show only a single resonance, indicating that there is no proton attached to the P atom. However, the $^{11}B\{^{1}H\}$ and ^{11}B spectra of compound **8** exhibit a singlet and a doublet at δ 22.2 ppm, indicating that a proton is attached to the boron atom. The signal of this proton was observed at δ 5.29 ppm in the ^{1}H NMR spectrum. **1** can also react with HBcat to give **16** in 85% yield, and the NMR spectra are similar to those of **8**. Consistent with the theoretical calculations, only the two B−O bond activated product was observed in the reactions of **1** with HBpin or HBcat. Attempts to trap the possible intermediate, such as compound **6** in Figure 1, were unsuccessful.

The structure of **8** was confirmed by high-resolution mass spectrometry (HRMS) and single-crystal X-ray diffraction.[62] As shown in Figure 6, the P atom in **8** exhibits a triangular-pyramidal geometry, which is different from the C_s configuration of the phosphorus center in compound **1**. However, the formation of compound **8** requires cleavage of two B−O bonds and formation of new B−N and B−O bonds. In this reaction, compound **1** exhibits a reaction mode different from that of the pincer-type phosphorus compound bearing a $[NNN]^{3-}$ ligand, which preferably activates the B−H bond in HBpin.[38] The activation of the B−O bond is particularly uncommon; there are only a few examples of B−O bond activation promoted by main-group elements[63,64] or rare-earth metals and transition-metal species.[65,66]

In order to further explore the selectivity of compound **1** to B−E bond activation, we examined the reaction of **1** with substrates containing both B−O and B−C or B−B bonds. As shown in Scheme 2, compound **1** reacts with pyrimidine-5-boronic acid pinacol ester and 2-fluoropyridine-4-boronic acid pinacol, producing **17** and **18** in 73% and 82% isolated yields, respectively. In addition, from a mixture of **1** with diboronic acid pinacol ester and biscatechol boronate, the two B−O bond activated products **19** and **20** were isolated. Unfortunately, attempts to react either **19** or **20** with compound **1** were unsuccessful, probably due to the greater steric hindrance of **19** and **20**. The new species (**19** and **20**) were fully characterized by NMR spectroscopy and HRMS (see the Supporting Information). Their NMR spectra are very similar to those of **8** and **16**, suggesting that these species have a structure similar to those formed by the B−O bond cleavage, whereas the B−B and B−C bonds in the substrates were unreactive.

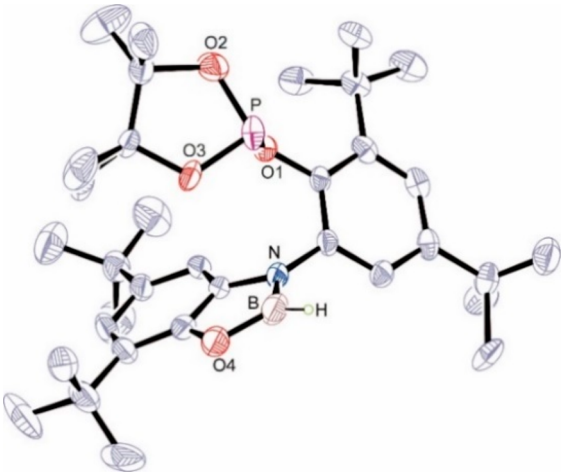

Figure 6. Molecular structure of **8** with thermal ellipsoids at the 50% probability level by X-ray diffraction. Hydrogen atoms on carbon are omitted for clarity.

The molecular structures of **18** and **20** were further confirmed by single-crystal X-ray diffraction (Figure 7). The most salient feature of **18** is the triangular-pyramidal phosphorus center, which is connected to three oxygen atoms. The newly formed B−O and B−N bonds are in the same plane as the 2-fluoropyridine-4-boron moiety and the benzene ring of the ligand. As in the structures of **8** and **18**, the phosphorus atom in **20** adopts a triangular-pyramidal configuration with a bond angle total of 290.57°, which is smaller than those in **8** (296.16°) and **18** (296.52°). The six atoms N, B1, O4, B2, O5, and O6 in compound **20** are noncoplanar, probably due to excessive steric repulsion. The formation of these products clearly proceeds through the cleavage of two B−O bonds. No B−H, B−B, or B−C bond cleavage products were observed, even at higher temperatures. Therefore, **1** is more reactive with a stronger B−O bond in comparison to species containing B−H, B−B, or B−C bonds.

The selective activation of the B−O bond to form **17** and **19** was investigated by DFT calculations. As illustrated in Table 2, the $\Delta G^{\circ\ddagger}$ values for the activation of B−O bonds by compound **1** are 19.7 and 20.6 kcal mol^{-1}, which are lower than those of the corresponding B−C (24.6 kcal mol^{-1}) and B−B (30.4 kcal mol^{-1}) bonds. Moreover, the $\Delta G^{\circ\ddagger}$ values for the activation of B−C and B−B bonds by compound **2** are 21.4 and 21.1 kcal mol^{-1}, which are lower than those of the corresponding B−O (33.6 and 29.4 kcal mol^{-1}, respectively) bond. This is consistent with the result that compound **1** with a $[ONO]^{3-}$ ligand prefers to activate the stronger B−O bond, while compound **2** with $[NNN]^{3-}$ prefers to activate the weaker B−B and B−C bonds (see Figures S7−S10 for more details).

CONCLUSION

In this work, theoretical calculations show that two different pincer-type phosphorus(III) compounds (**1** and **2**) exhibit different reaction modes when they are confronted with the

https://dx.doi.org/10.1021/acs.inorgchem.0c01920
Inorg. Chem. 2020, 59, 15636−15645

Scheme 2. B−O Bond Activation by 1 in the Presence of B−B or B−C Bonds

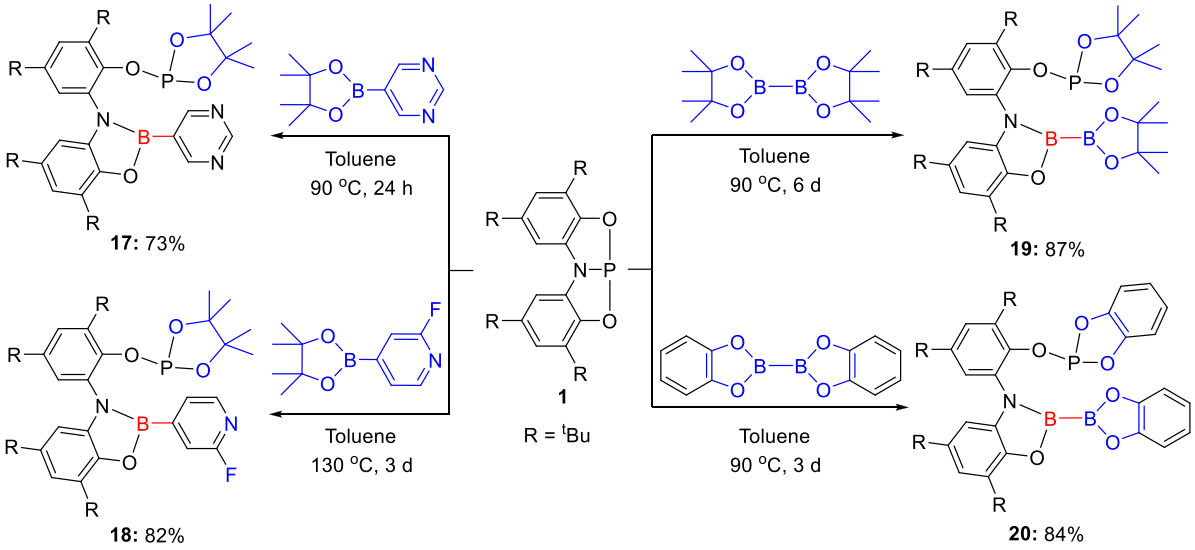

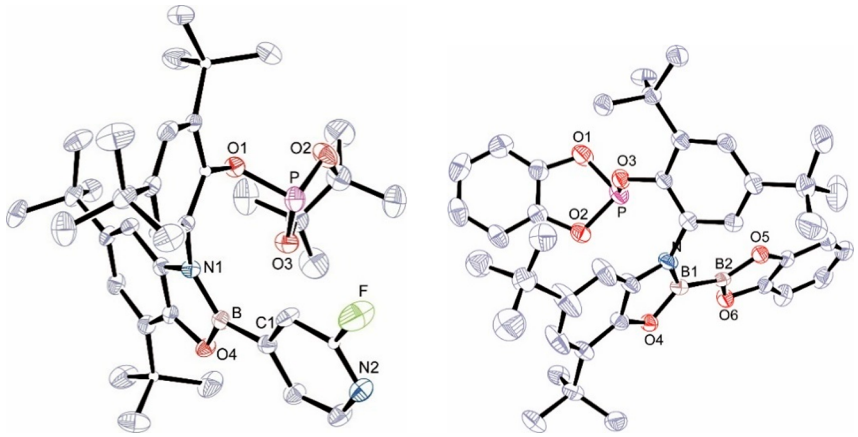

Figure 7. Molecular structures of **18** (left) and **20** (right) with thermal ellipsoids at the 50% probability level by X-ray diffraction. Hydrogen atoms on carbon are omitted for clarity.

Table 2. $\Delta G^{\circ\ddagger}$ and ΔG° Values for the Activation of B−C, B−B, and B−O Bonds by Compounds 1 and 2[a]

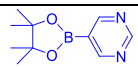

	$\Delta G^{\circ\ddagger}$(B-C)	ΔG°(B-C)	$\Delta G^{\circ\ddagger}$(B-O)	ΔG°(B-O)
1	24.6	-13.4	19.7	-7.7
2	21.4	-9.2	33.6	-1.4

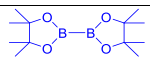

	$\Delta G^{\circ\ddagger}$(B-B)	ΔG°(B-B)	$\Delta G^{\circ\ddagger}$(B-O)	ΔG°(B-O)
1	30.4	-19.6	20.6	-7.2
2	21.1	-14.0	29.4	-4.4

[a]The Gibbs energies are given in kcal mol^{-1}.

same substrate. The former, with an $[ONO]^{3-}$ ligand, prefers selective activation of the B−O bond over the weaker B−H, B−B, or B−C bonds in a variety of pinacol- and catechol-ligated boron compounds, and this was confirmed experimentally. In contrast, compound **2**, with a $[NNN]^{3-}$ ligand, prefers cleavage of B−H, B−B, or B−C bonds over cleavage of the B−O bond. The origin of the chemoselectivity of the B−O bond cleavage by compound **1** is the charge transfer, which is stronger than those involved in the B−H bond cleavage. This is because the HOMO−LUMO gap for the B−O bond in **1** is smaller. Experimentally, compound **8** was isolated by the reaction of compound **1** with HBpin. If the B−H bond in the borane substrate changes to a B−C or B−B bond, the chemoselectivity of B−O bond cleavage was retained.

■ ASSOCIATED CONTENT

Supporting Information

The Supporting Information is available free of charge at https://pubs.acs.org/doi/10.1021/acs.inorgchem.0c01920.

Experimental procedures and analytical data (^{1}H, ^{31}P and ^{13}C NMR, HRMS) for all new compounds (PDF)

Cartesian coordinates for the calculated structures (XYZ)

Accession Codes

CCDC 1990625−1990627 contain the supplementary crystallographic data for this paper. These data can be obtained free of charge via www.ccdc.cam.ac.uk/data_request/cif, or by email-

https://dx.doi.org/10.1021/acs.inorgchem.0c01920
Inorg. Chem. 2020, 59, 15636−15645

ing data_request@ccdc.cam.ac.uk, or by contacting The Cambridge Crystallographic Data Centre, 12 Union Road, Cambridge CB2 1EZ, UK; fax: +44 1223 336033.

AUTHOR INFORMATION

Corresponding Authors

Jun Zhu − *State Key Laboratory of Physical Chemistry of Solid Surfaces and Collaborative Innovation Center of Chemistry for Energy Materials (iChEM), and Department of Chemistry, College of Chemistry and Chemical Engineering, Xiamen University, Xiamen 361005, People's Republic of China;* orcid.org/0000-0002-2099-3156; Email: jun.zhu@xmu.edu.cn

Congqing Zhu − *State Key Laboratory of Coordination Chemistry, Jiangsu Key Laboratory of Advanced Organic Materials, School of Chemistry and Chemical Engineering, Nanjing University, Nanjing 210093, People's Republic of China;* orcid.org/0000-0003-4722-0484; Email: zcq@nju.edu.cn

Guixiang Zeng − *Kuang Yaming Honors School, Institute for Brain Sciences, Nanjing University, Nanjing 210093, People's Republic of China;* orcid.org/0000-0001-5519-7611; Email: gxzeng@nju.edu.cn

Authors

Qin Zhu − *Kuang Yaming Honors School, Institute for Brain Sciences, Nanjing University, Nanjing 210093, People's Republic of China; State Key Laboratory of Physical Chemistry of Solid Surfaces and Collaborative Innovation Center of Chemistry for Energy Materials (iChEM), and Department of Chemistry, College of Chemistry and Chemical Engineering, Xiamen University, Xiamen 361005, People's Republic of China*

Penglong Wang − *State Key Laboratory of Coordination Chemistry, Jiangsu Key Laboratory of Advanced Organic Materials, School of Chemistry and Chemical Engineering, Nanjing University, Nanjing 210093, People's Republic of China*

Complete contact information is available at: https://pubs.acs.org/10.1021/acs.inorgchem.0c01920

Author Contributions

‖Q.Z. and P.W. contributed equally.

Notes

The authors declare no competing financial interest.

ACKNOWLEDGMENTS

This research was supported by the National Natural Science Foundation of China (Grant Nos. 21772088 and 21703098), the Natural Science Foundation of Jiangsu Province (Grant No. BK20170635), the Young Elite Scientist Sponsorship Program of China Association of Science and Technology, the program of Jiangsu Specially-Appointed Professor, Shuangchuang Talent Plan of Jiangsu Province, and the Fundamental Research Funds for the Central Universities (14380009 and 14380010). Calculations were performed using computational resources on an IBM Blade cluster system from the High Performance Computing Center (HPCC) of Nanjing University.

REFERENCES

(1) Li, C. J. Cross-Dehydrogenative Doupling (CDC): Exploring C-C Bond Formations Beyond Functional Group Transformations. *Acc. Chem. Res.* **2009**, *42*, 335−344.

(2) Sun, C. L.; Li, B. J.; Shi, Z. J. Direct C-H Transformation via Iron Catalysis. *Chem. Rev.* **2011**, *111*, 1293−1314.

(3) Mesganaw, T.; Garg, N. K. Ni- and Fe-Catalyzed Cross-Coupling Reactions of Phenol Derivatives. *Org. Process Res. Dev.* **2013**, *17*, 29−39.

(4) Yamaguchi, J.; Yamaguchi, A. D.; Itami, K. C-H Bond Functionalization: Emerging Synthetic Tools for Natural Products and Pharmaceuticals. *Angew. Chem., Int. Ed.* **2012**, *51*, 8960−9009.

(5) Bolm, C.; Legros, J.; Le Paih, J.; Zani, L. Iron-Catalyzed Reactions in Organic Synthesis. *Chem. Rev.* **2004**, *104*, 6217−6254.

(6) Vastine, B. A.; Hall, M. B. The Molecular and Electronic Structure of Carbon−Hydrogen Bond Activation and Transition Metal Assisted Hydrogen Transfer. *Coord. Chem. Rev.* **2009**, *253*, 1202−1218.

(7) Shi, Z.; Zhang, C.; Tang, C.; Jiao, N. Recent Advances in Transition-Metal Catalyzed Reactions using Molecular Oxygen as the Oxidant. *Chem. Soc. Rev.* **2012**, *41*, 3381−3430.

(8) Shang, R.; Ilies, L.; Nakamura, E. Iron-Catalyzed C-H bond Activation. *Chem. Rev.* **2017**, *117*, 9086−9139.

(9) Power, P. P. Main-group Elements as Transition Metals. *Nature* **2010**, *463*, 171−177.

(10) Coyle, E. E.; O'brien, C. J. Main Group Chemistry: Bonsai Phosphorus. *Nat. Chem.* **2012**, *4*, 779−780.

(11) Chu, T.; Nikonov, G. I. Oxidative Addition and Reductive Elimination at Main-group Element Centers. *Chem. Rev.* **2018**, *118*, 3608−3680.

(12) Melen, R. L. Frontiers in Molecular p-Block Chemistry: From Structure to Reactivity. *Science* **2019**, *363*, 479−484.

(13) Tonner, R.; Öxler, F.; Neumüller, B.; Petz, W.; Frenking, G. Carbodiphosphoranes: The Chemistry of Divalent Carbon(0). *Angew. Chem., Int. Ed.* **2006**, *45*, 8038−8042.

(14) Dyker, C. A.; Lavallo, V.; Donnadieu, B.; Bertrand, G. Synthesis of an Extremely Bent Acyclic Allene (a "Carbodicarbene"): A Strong Donor Ligand. *Angew. Chem., Int. Ed.* **2008**, *47*, 3206−3209.

(15) Frenking, G.; Tonner, R.; Klein, S.; Takagi, N.; Shimizu, T.; Krapp, A.; Pandey, K. K.; Parameswaran, P. New Bonding Modes of Carbon and Heavier Group 14 Atoms Si-Pb. *Chem. Soc. Rev.* **2014**, *43*, 5106−5139.

(16) Chen, W.-C.; Lee, C.-Y.; Lin, B.-C.; Hsu, Y.-C.; Shen, J.-S.; Hsu, C.-P.; Yap, G. P. A.; Ong, T.-G. The Elusive Three-Corrdinate Dicationic Hydride Boron Complex. *J. Am. Chem. Soc.* **2014**, *136*, 914−917.

(17) Roy, S.; Mondal, K. C.; Roesky, H. W. Cyclic Alkyl(amino) Carbene Stabilized Complexes with Low Coordinate Metals of Enduring Nature. *Acc. Chem. Res.* **2016**, *49*, 357−369.

(18) Zhu, Z.; Wang, X.; Peng, Y.; Lei, H.; Fettinger, J. C.; Rivard, E.; Power, P. P. Addition of Hydrogen or Ammonia to a Low-Valent Group 13 Metal Species at 25 °C and 1 atm. *Angew. Chem., Int. Ed.* **2009**, *48*, 2031−2034.

(19) Protchenko, A. V.; Birjkumar, K. H.; Dange, D.; Schwarz, A. D.; Vidovic, D.; Jones, C.; Kaltsoyannis, N.; Mountford, P.; Aldridge, S. A stable Two-coordinate Acyclic Silylene. *J. Am. Chem. Soc.* **2012**, *134*, 6500−6503.

(20) Gellrich, U.; Diskin-Posner, Y.; Shimon, L. J.; Milstein, D. Reversible Aromaticity Transfer in a Bora-Cycle: Boron-Ligand Cooperation. *J. Am. Chem. Soc.* **2016**, *138*, 13307−13313.

(21) Hicks, J.; Vasko, P.; Goicoechea, J. M.; Aldridge, S. Synthesis, Structure and Reaction Chemistry of a Nucleophilic Aluminyl Anion. *Nature* **2018**, *557*, 92−95.

(22) Légaré, M. A.; Rang, M.; Bélanger-Chabot, G.; Schweizer, J. I.; Krummenacher, I.; Bertermann, R.; Arrowsmith, M.; Holthausen, M. C.; Braunschweig, H. The Reductive Coupling of Dinitrogen. *Science* **2019**, *363*, 1329−1332.

(23) Stephan, D. W.; Erker, G. Frustrated Lewis Pairs: Metal-free Hydrogen Activation and More. *Angew. Chem., Int. Ed.* **2010**, *49*, 46−76.

(24) Stephan, D. W. Frustrated Lewis Pairs: From Concept to Catalysis. *Acc. Chem. Res.* **2015**, *48*, 306−316.

(25) Kehr, G.; Erker, G. Frustrated Lewis Pair Chemistry: Searching for New Reactions. *Chem. Rec.* **2017**, *17*, 803−815.

(26) Lam, J.; Szkop, K. M.; Mosaferi, E.; Stephan, D. W. FLP Catalysis: Main Group Hydrogenations of Organic Unsaturated Substrates. *Chem. Soc. Rev.* **2019**, *48*, 3592−3612.

(27) Culley, S. A.; Arduengo, A. J., III Synthesis and Structure of the First 10-P-3 Species. *J. Am. Chem. Soc.* **1984**, *106*, 1164−1165.
(28) Arduengo, A. J., III; Stewart, C. A.; Davidson, F.; Dixon, D. A.; Becker, J. Y.; Culley, S. A.; Mizen, M. B. The Synthesis, Structure, and Chemistry of 10-Pn-3 Systems: Tricoordinate Hypervalent Pnicogen Compounds. *J. Am. Chem. Soc.* **1987**, *109*, 627−647.
(29) Cui, J.; Li, Y.; Ganguly, R.; Inthirarajah, A.; Hirao, H.; Kinjo, R. Metal-free σ-bond Metathesis in Ammonia Activation by a Diazadiphosphapentalene. *J. Am. Chem. Soc.* **2014**, *136*, 16764−16767.
(30) Cui, J.; Li, Y.; Ganguly, R.; Kinjo, R. Reactivity Studies on a Diazadiphosphapentalene. *Chem. - Eur. J.* **2016**, *22*, 9976−9985.
(31) Robinson, T. P.; De Rosa, D. M.; Aldridge, S.; Goicoechea, J. M. E-H Bond Activation of Ammonia and Water by a Geometrically Constrained Phosphorus(III) Compound. *Angew. Chem., Int. Ed.* **2015**, *54*, 13758−13763.
(32) Robinson, T. P.; Lo, S. K.; De Rosa, D.; Aldridge, S.; Goicoechea, J. M. On the Ambiphilic Reactivity of Geometrically Constrained Phosphorus(III) and Arsenic(III) Compounds: Insights into Their Interaction with Ionic Substrates. *Chem. - Eur. J.* **2016**, *22*, 15712−15724.
(33) Robinson, T. P.; De Rosa, D.; Aldridge, S.; Goicoechea, J. M. On the Redox Reactivity of a Geometrically Constrained Phosphorus(III) Compound. *Chem. - Eur. J.* **2017**, *23*, 15455−15465.
(34) Dunn, N. L.; Ha, M.; Radosevich, A. T. Main Group Redox Catalysis: Reversible P^{III}/P^{V} Redox Cycling at a Phosphorus Platform. *J. Am. Chem. Soc.* **2012**, *134*, 11330−11333.
(35) McCarthy, S. M.; Lin, Y. C.; Devarajan, D.; Chang, J. W.; Yennawar, H. P.; Rioux, R. M.; Ess, D. H.; Radosevich, A. T. Intermolecular N-H Oxidative Addition of Ammonia, Alkylamines, and Arylamines to a Planar σ^3-Phosphorus Compound via an Entropy-Controlled Electrophilic Mechanism. *J. Am. Chem. Soc.* **2014**, *136*, 4640−4650.
(36) Zhao, W.; McCarthy, S. M.; Lai, T. Y.; Yennawar, H. P.; Radosevich, A. T. Reversible Intermolecular E-H Oxidative Addition to a Geometrically Deformed and Structurally Dynamic Phosphorous Triamide. *J. Am. Chem. Soc.* **2014**, *136*, 17634−17644.
(37) Reichl, K. D.; Dunn, N. L.; Fastuca, N. J.; Radosevich, A. T. Biphilic Organophosphorus Catalysis: Regioselective Reductive Transposition of Allylic Bromides via P^{III}/P^{V} Redox Cycling. *J. Am. Chem. Soc.* **2015**, *137*, 5292−5295.
(38) Lin, Y. C.; Hatzakis, E.; McCarthy, S. M.; Reichl, K. D.; Lai, T. Y.; Yennawar, H. P.; Radosevich, A. T. P-N Cooperative Borane Activation and Catalytic Hydroboration by a Distorted Phosphorous Triamide Platform. *J. Am. Chem. Soc.* **2017**, *139*, 6008−6016.
(39) Murillo, A.; Chiquete, L. M.; Josephnathan, P.; Contreras, R. Syntheses and Reactivity of New PH Dibenzobicyclic Phosphoranes bearing Hydroxy-, Alkoxy-, Oxo-, Amido-, and Dihydrido-functions at the Phosphorus Atom. *Phosphorus, Sulfur Silicon Relat. Elem.* **1990**, *53*, 87−101.
(40) Driess, M.; Muresan, N.; Merz, K.; Päch, M. Formation of a Bowl-Shaped, Pentacyclic Phosphonium Cage by Methylation of a Nucleophilic Phosphinidene. *Angew. Chem., Int. Ed.* **2005**, *44*, 6734−6737.
(41) Volodarsky, S.; Dobrovetsky, R. Ambiphilic Geometrically Constrained Phosphenium Cation. *Chem. Commun.* **2018**, *54*, 6931−6934.
(42) Hentschel, A.; Brand, A.; Wegener, P.; Uhl, W. A Sterically Constrained Tricyclic PC_3 Phosphine: Coordination Behavior and Insertion of Chalcogen Atoms into P-C Bonds. *Angew. Chem., Int. Ed.* **2018**, *57*, 832−835.
(43) Brand, A.; Uhl, W. Sterically Constrained Bicyclic Phosphines: A Class of Fascinating Compounds Suitable for Application in Small Molecule Activation and Coordination Chemistry. *Chem. - Eur. J.* **2019**, *25*, 1391−1404.
(44) Burgess, K.; Ohlmeyer, M. Transition-Metal Promoted Hydroborations of Alkenes, Emerging Methodology for Organic Transformations. *Chem. Rev.* **1991**, *91*, 1179−1191.
(45) Neeve, E. C.; Geier, S. J.; Mkhalid, I. A.; Westcott, S. A.; Marder, T. B. Diboron(4) Compounds: From Structural Curiosity to Synthetic Workhorse. *Chem. Rev.* **2016**, *116*, 9091−9161.
(46) Yoshida, H. Borylation of Alkynes under Base/Coinage Metal Catalysis: Some Recent Developments. *ACS Catal.* **2016**, *6*, 1799−1811.
(47) Prieschl, D.; Belanger-Chabot, G.; Guo, X.; Dietz, M.; Muller, M.; Krummenacher, I.; Lin, Z.; Braunschweig, H. Synthesis of Complex Boron-Nitrogen Heterocycles Comprising Borylated Triazenes and Tetrazenes Under Mild Conditions. *J. Am. Chem. Soc.* **2020**, *142*, 1065−1076.
(48) Zeng, G.; Maeda, S.; Taketsugu, T.; Sakaki, S. Catalytic Hydrogenation of Carbon Dioxide with Ammonia-Borane by Pincer-Type Phosphorus Compounds: Theoretical Prediction. *J. Am. Chem. Soc.* **2016**, *138*, 13481−13484.
(49) Zeng, G.; Maeda, S.; Taketsugu, T.; Sakaki, S. Theoretical Study of Hydrogenation Catalysis of Phosphorus Compound and Prediction of Catalyst with High Activity and Wide Application Scope. *ACS Catal.* **2016**, *6*, 4859−4870.
(50) Becke, A. D. Density-Functional Exchange-Energy Approximation with Correct Asymptotic Behavior. *Phys. Rev. A: At., Mol., Opt. Phys.* **1988**, *38*, 3098−3100.
(51) Becke, A. D. Density-Functional Thermochemistry. III. The Role of Exact Exchange. *J. Chem. Phys.* **1993**, *98*, 5648−5652.
(52) Grimme, S.; Antony, J.; Ehrlich, S.; Krieg, H. A Consistent and Ac-curate Ab Initio Parametrization of Density Functional Dispersion Correction (DFT-D) for the 94 Elements H-Pu. *J. Chem. Phys.* **2010**, *132*, 154104.
(53) Barone, V.; Cossi, M. Quantum Calculation of Molecular Energies and Energy Gradients in Solution by a Conductor Solvent Model. *J. Phys. Chem. A* **1998**, *102*, 1995−2001.
(54) Tomasi, J.; Mennucci, B.; Cammi, R. Quantum Mechanical Continuum Solvation Models. *Chem. Rev.* **2005**, *105*, 2999−3094.
(55) Fukui, K. Formulation of the Reaction Coordinate. *J. Phys. Chem.* **1970**, *74*, 4161−4163.
(56) Fukui, K. The Path of Chemical Reactions-the IRC Approach. *Acc. Chem. Res.* **1981**, *14*, 363−368.
(57) Ditchfield, R.; Hehre, W. J.; Pople, J. A. Self-Consistent Molecular-Orbital Methods. IX. An Extended Gaussian-Type Basis for Molecular-Orbital Studies of Organic Molecules. *J. Chem. Phys.* **1971**, *54*, 724−728.
(58) Clark, T.; Chandrasekhar, J.; Spitznagel, G. W.; Schleyer, P. v. R. Efficient Diffuse Function- Augmented Basis Sets for Anion Calculations. III. The 3-21+ G Basis Set for First-Row Elements, Li-F. *J. Comput. Chem.* **1983**, *4*, 294−301.
(59) Hariharan, P. C.; Pople, J. A. The Influence of Polarization Functions on Molecular Orbital Hydrogenation Energies. *Theoretica Chimica Acta* **1973**, *28*, 213−222.
(60) Frisch, M. J.; Trucks, G. W.; Schlegel, H. B.; Scuseria, G. E.; Robb, M. A.; Cheeseman, J. R.; Scalmani, G.; Barone, V.; Petersson, G. A.; Nakatsuji, H.; Li, X.; Caricato, M.; Marenich, A. V.; Bloino, J.; Janesko, B. G.; Gomperts, R.; Mennucci, B.; Hratchian, H. P.; Ortiz, J. V.; Izmaylov, A. F.; Sonnenberg, J. L.; Williams-Young, D.; Ding, F.; Lipparini, F.; Egidi, F.; Goings, J.; Peng, B.; Petrone, A.; Henderson, T.; Ranasinghe, D.; Zakrzewski, V. G.; Gao, J.; Rega, N.; Zheng, G.; Liang, W.; Hada, M.; Ehara, M.; Toyota, K.; Fukuda, R.; Hasegawa, J.; Ishida, M.; Nakajima, T.; Honda, Y.; Kitao, O.; Nakai, H.; Vreven, T.; Throssell, K.; Montgomery, J. A., Jr.; Peralta, J. E.; Ogliaro, F.; Bearpark, M. J.; Heyd, J. J.; Brothers, E. N.; Kudin, K. N.; Staroverov, V. N.; Keith, T. A.; Kobayashi, R.; Normand, J.; Raghavachari, K.; Rendell, A. P.; Burant, J. C.; Iyengar, S. S.; Tomasi, J.; Cossi, M.; Millam, J. M.; Klene, M.; Adamo, C.; Cammi, R.; Ochterski, J. W.; Martin, R. L.; Morokuma, K.; Farkas, O.; Foresman, J. B.; Fox, D. J. *Gaussian 16, Rev. A.03*; Gaussian, Inc.: Wallingford, CT, USA, 2016.
(61) Dapprich, S.; Frenking, G. Investigation of Donor-Acceptor Interac-tions: A Charge Decomposition Analysis Using Fragment Molecular Orbitals. *J. Phys. Chem.* **1995**, *99*, 9352−9362.
(62) CCDC 1990626 (**8**), 1990625 (**18**), and 1990627 (**20**) contain the crystallographic data for this paper.

https://dx.doi.org/10.1021/acs.inorgchem.0c01920
Inorg. Chem. 2020, 59, 15636−15645

(63) Westcott, S. A.; Blom, H. P.; Marder, T. B.; Baker, R. T.; Calabrese, J. C. Nucleophile Promoted Degradation of Catecholborane: Consequences for Transition Metal-Catalyzed Hydroborations. *Inorg. Chem.* **1993**, *32*, 2175−2182.
(64) Eichhorn, A. F.; Fuchs, S.; Flock, M.; Marder, T. B.; Radius, U. Reversible Oxidative Addition at Carbon. *Angew. Chem., Int. Ed.* **2017**, *56*, 10209−10213.
(65) Wang, W.; Lv, Y.; Gou, X.; Leng, X.; Chen, Y. Boron-Oxygen Bond Cleavage of Pinacolborane and Catecholborane Mediated by a Scandium Phosphinidene Complex. *Chin. J. Chem.* **2014**, *32*, 752−756.
(66) Chu, J.; Wang, C.; Xiang, L.; Leng, X.; Chen, Y. Reactivity of Scandium Terminal Imido Complex toward Boranes: C(sp^3)-H Bond Borylation and B-O Bond Cleavage. *Organometallics* **2017**, *36*, 4620−4625.

https://dx.doi.org/10.1021/acs.inorgchem.0c01920
Inorg. Chem. 2020, 59, 15636−15645